Structural Analysis and Validation of a Smart Pantograph Mast Concept

Branko Glisic*, Sigrid Adriaenssens & Peter Szerzo

Department of Civil and Environmental Engineering, Princeton University, Princeton, NJ, USA

Abstract: *To progress the development of deployable, lightweight infrastructure for relief and recovery efforts in the aftermath of natural and man-made disasters, this article develops a proof of concept for a smart mast that leverages the versatility of pantograph systems and advances in sensor, actuator, and informatics technologies. More specifically the article addresses key design criteria of transportability, deployability, global stability, and site responsiveness through the development of analytical expressions and control framework, and reduced-scale physical model testing. The case study, a three-tiered tetrahedral mast is composed of three connected sets of planar pantograph systems and deployed by single actuator located between two of the three mast supports. The article discusses the optimum configurations for the individual design criteria and trade-offs to be made between compactness, overturning, and operational power. The design, construction, and experimentation with a 73-cm tall fully deployed physical model reinforce the feasibility of the presented smart mast concept.*

1 INTRODUCTION

The occurrence of extreme natural and man-made disasters in densely populated areas shows the need to improve relief and recovery infrastructure. Adaptable infrastructure that is compact and rapidly deployed in the field is critical for an effective humanitarian response. For example wind turbines mounted on a deployable mast can provide a vital energy supply system while functioning independently of a damaged or inadequate existing electricity grid. The deployability and compatibility exhibited in systems such as the "Power in a Box" design (Peters, 2012) with its telescoping mast and top mounted wind turbines (shown in Figure 1) has been a point of reference for this article.

To whom correspondence should be addressed. E-mail: bglisic@princeton.edu.

Typical masts that support wind turbines have a very narrow body braced by guy lines. This system has two major disadvantages in a disaster relief context: (1) the mast's height is fixed and mostly limited by dead load and the maximum wind speed; as a consequence the mast cannot adapt its shape to tap into the desirable wind speeds available at varying heights; and (2) the anchoring distance of the guy lines is typically in the order of 65% of the mast height (Ghodrati, 2002). Although the mast might be very slender its bracing system takes up a large part of a site that might not be available in the context of a dense damaged urban fabric. In summary, the main challenges related to the use of masts with turbines in urban areas struck by disaster are transportability, rapid deployability, responsiveness (adaptability), and global stability. A compact, adaptive, and stable mast can be a good solution addressing all these challenges.

This article gives a proof of concept through the development and exploration of analytical expressions and a physical model of a smart pantograph mast that does not impinge upon the surrounding area and that changes its shape in reaction to varying external stimuli.

1.1 Overview of civil smart and pantograph structures

Systems equipped with sensors, actuators, and processing capabilities that actively adapt to changing external conditions (such as loading) have been described as smart, adaptive, or active (Ching et al., 2008). The design and analysis of smart structures is particularly advanced in the aerospace and space technology sector, for example, morphing wings (Moorhouse et al., 2006), deployable space structures (Jiang-Pin and Dong-Xu, 2010), etc. This article focuses on smart civil structural engineering systems where although several studies were undertaken (e.g., Del Grosso and Basso, 2011) less real applications exist, mostly limited to the use of

Fig. 1. (Left) Physical model; (middle and right) full-scale prototype for "Power in a Box," a telescoping mast with a wind turbine mounted on a transportable standard steel shipping container ("Power in a Box," Princeton University; middle photo courtesy of Catherine Peters; right photo courtesy of Frank Wojciechowski).

semiactive or active control devices in earthquake engineering (e.g., Bitaraf et al., 2012, Aldemir, 2010).

The term kinetic architecture was pioneered into the structural engineering domain by Zuk and Clark (1970). They introduced the concept of biomimetic smart structures that fold, expand, and contract to adjust to changing spatial requirements. Initial research on active structural control in tall building design by Yao (1972) is important in the context of this article. His work hinted at how tall smart buildings/masts could adapt their behavior in reaction to external variations in loading. This responsiveness presents an opportunity to keep all structural behavior with the limit state criteria but also to actively change geometry to avoid, deflect, or attract more external loading stimuli.

The recent advent of new sensor and actuator technologies combined with the advances in structural lightweight design and increased computational capacity creates a favorable climate for the development of smart civil structures. The main research and industrial smart structural design endeavors undertaken recently are reported as follows. Pawlowski and Holnikci-Szulc (2004) designed and tested a sensor equipped structure that detects impact under extreme loads and redistributes internal loading. Hunt et al. (2009) developed a design tool that generates structural systems that vary local stiffness to globally counteract the effect of unexpected loads. Noak et al. (2006) experimentally integrated actuators in trussed beams and achieved increasing spans and load bearing capacity. Adriaenssens and Ney (2007) advocated integrating the actuator as a structural element in realized mobile vehicular bridges. Saleh and Adeli (1998) explored the algorithms for

control of adaptable smart structures, while Kim and Adeli developed and tested various robust algorithms for structural control based on advanced statistical and analytical methods (e.g., Kim and Adeli, 2004, 2005a, b). Most recently active tensegrity systems have been researched that use control of self-stress to actively manipulate their static and dynamic behavior (Adam and Smith, 2008).

As pantograph or scissor-hinged systems can be equipped with active elements, they have the potential to adapt to their environment. A recent in-depth overview of pantograph systems is given in Thrall (2011). Pantographs are a specific type of deployable structures that deploy from a small compact state to another one while carrying loads. Gantes (2001) defined four categories of deployable structures: (1) assemblies of one-dimensional rigid bars that form a pantograph (also called linkage or scissor element), (2) assemblies of rigid two-dimensional plates, (3) tensile structures (including cable, membrane, and pneumatic systems), and (4) tensegrity structures (assemblies of nontouching compression struts surrounded by a tensile network). This article focuses on the first category and more specifically the pantograph mast.

A pantograph or scissor-like element consists of three noded rigid bars (two nodes at the ends and one located between them) that are connected at their ends and at the intermediate node with a hinge. The pantograph system, initially conceived as an accurate drafting tool to scale line drawings, allows for significant decreases in height with increasing spans. When flat, the pantograph lattice (like a garden trellis) with its hinged connections is a mechanism with one degree of freedom.

If the lattice members are totally rigid and connected with frictionless joints, the movement of one member parallel to another causes sympathetic movement in the entire lattice. The first sketches of pantograph systems appear in Leonardo Da Vinci's 15th century notebooks (Escrig, 2001). Pinero (1965) patented the first three-dimensional deployable pantograph structure covering a medium span performance area. Based on Pinero's design, Zeigler (1976) arranged the same structural elements in a specific spherical, dome-like configuration that self-locks upon full deployment. Escrig (1985) developed a series of expandable space frames using pantographs and realized them as deployable sunroofs covering swimming pools. Both Pinero and Escrig used simple scissor elements: a pantograph with straight rods connected at an intermediate hinge. Studies that examine the main principles, the geometric properties, and the shape limitations of both planar and spatial structures made of pantograph elements with equal length beam and a centrally located intermediate hinge, have been carried out by Zhao et al. (2009, 2011) and Cai et al. (2012). Hoberman's (1990) patent describes an angulated element as building block of a hoop assembly. This element, realized in Iris Dome at the German Pavilion at the Expo 2000 Hanover, features identical kinked rods rather than straight rods. You and Pellegrino (1997) developed from this angulated element the generalized angulated element, an assembly of kinked rods, which when deployed embrace a constant angle. Pellegrino and Kwan (1991) and Kwan (2003) presented numerical simulations and a physical prototype of a pantograph mast, activated and stiffened by a network of cable segments and active cables. More recently Tan and Pellegrino presented a dynamic model for this cable-stiffened pantograph mast (Tan and Pellegrino, 2008). Formulations that describe the dynamic deployment equations of a pantograph mast were developed by Chen et al. (2002).

Applications and research of pantograph systems that change shape in reaction to external stimuli are few, small scale, and found outside the domain of civil structures in (1) high-speed transportation equipped with active dynamics control (Park et al., 2003), (2) artificial-legged auto-motion (Kar, 2003; Freedman, 1991), and (3) hand controllers for tele-operation (Long and Collins, 1992). To the best of the authors' knowledge, no smart tetrahedral pantograph structures under gravity and lateral loading have been researched, designed, and validated with a physical model.

1.2 Scope and design methodology

The overall aim of this research is to study a deployable, adaptable tetrahedral pantograph mast (in short smart mast) supporting wind turbines, to understand its structural and kinematic behavior and identify design challenges. As the mast is not designed to be deeply anchored to the soil, strong wind loading can affect its global stability. This phenomenon can be avoided by designing the mast to change its shape (i.e., to collapse to the lowest acceptable height that would guarantee global stability), while still enabling energy harvesting (by keeping the turbines in the wind).

The smart mast exhibits complex structural behavior. To achieve the overall aim of the project a step-by-step approach is adopted. The major fundamental questions on feasibility of such a structure and the proof of concept are addressed in this article (Step 1). This includes the studies on the change of shape under external influences, overall global stability requirements, structural analysis of the mast during the deployment, and a physical concept validation. Other aspects (e.g., detailed global stability under the wind, realization of details, power consumption, etc.) are considered as challenges imposed by realistic conditions at application level, and they will be addressed in future research (Step 2). This article thus presents the conceptual design and reduced-scale physical model validation of a smart pantograph mast supporting wind turbines that adapts its shape in response to the presence of the predominant wind speed. At this stage of the research, detailed dynamic analysis of the mast behavior, testing of the model in wind tunnel, and development of detailed algorithms for data analysis are considered as out of scope of the article. Based on the encouraging outcomes of the presented research, these matters are rather considered as the next stage in the research.

To keep the costs of the model minimal, the small-scale smart mast was equipped at different levels with in-house available fiber-optic (FO) temperature sensors, instead of wind pressure sensors. Applying hot air of a certain temperature to one of the sensors causes the mast to collapse to the exact height where the temperature increase occurred. The application of hot air simulates the application of the predominant wind that would occur in reality. This simplification does not affect the results or the conclusions of the presented research, since the numerical outputs are the same for temperature and wind pressure sensors (i.e., scalar value for each instrumented point). Once the proof of the concept is established in this article, more sophisticated sensing systems for the mast could be designed based not only on FO pressure sensors (Pinet et al., 2007), but also on FO strain or displacement sensors (Glisic et al., 2007; Inaudi et al., 2001). The preference for FO sensors is based on their proven accuracy, resolution, versatility, and long-term stability (Inaudi and Glisic, 2002, 2006; Glisic and Inaudi, 1999).

Fig. 2. Conceptual rendering of the three-dimensional tetrahedral pantograph mast.

2 CONCEPTUAL DESIGN OF THE PANTOGRAPH MAST

2.1 Geometrical properties

In this section, the kinematic analytical concept of the deployable mast is presented. The three-dimensional tetrahedral mast is assembled of three inclined two-dimensional planar pantograph systems, as shown in Figure 2.

The tetrahedral overall shape is preferred over a prismatic shape as the former offers improved global stability against overturning (e.g., due to wind). The analytical formulation that describes the geometry and more specifically the positions of the end and intermediate nodes of the two-dimensional straight rod pantographs in all phases of shape change is presented as follows.

The planar systems are assembled into a three-dimensional mast by connecting their end nodes. To limit stresses on those end nodes, their hinges (indicated in Figure 3 by notations A, B, C, and D) must be collinear during all deployment stages. Consequently, each pantograph is symmetric with respect to the vertical axis as shown in Figure 3.

Any geometric deviations of the end hinges from collinear arrangement, increases fatigue damage in the hinges after several cycles of elongation and contraction of the mast. Analytically this required collinear geometric condition is fulfilled if

$$c_n = c_{n-1} = \cdots = c_i \cdots = c_1 \tag{1}$$

and

$$l_i = \frac{1 - c_{i-1}}{c_i} l_{i-1} = \left(\frac{1 - c_1}{c_1} \right)^{i-1} l_1 \tag{2}$$
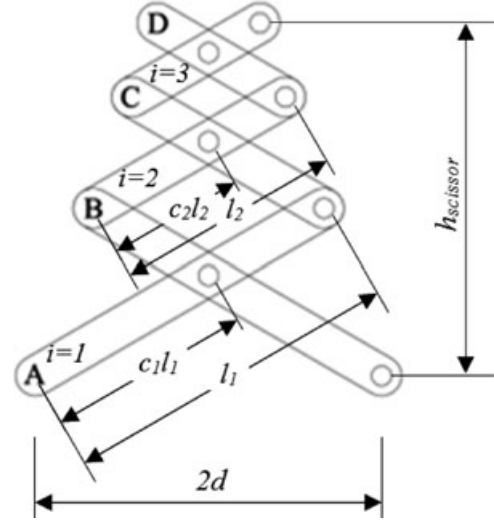

Fig. 3. Schematic representation of a two-dimensional planar pantograph whose end hinges A, B, C, and D must be collinear during the entire deployment process.

where l_i is the length between the two end nodes of the ith scissor element, c_i is the ratio of the length between the bottom end node and the intermediate node to the length between the two end nodes of the ith scissor element ($i = 2, \ldots n$, see Figure 3).

The value of c_1 must be higher than 0.5 that is, $(1 - c_1)/ c_1 < 1$. For $c_1 < 0.5$ the overall shape of the mast is an upside-down tetrahedron, while for $c_1 = 0.5$ the overall shape is prismatic. Thus, for $c_1 > 0.5$, Equation (2) describes the decreasing lengths of the scissor elements in successive order and indicates that the portion above the hinge of the $(i - 1)$th element is equal to the portion below the hinge of the ith element. If the total number of different elements is n, then sum of the lengths of n different elements L_n can be calculated using Equations (3a and b)

$$L_n = \sum_{i=1}^{n} l_i = \sum_{i=1}^{n} \left(\frac{1 - c_1}{c_1} \right)^{i-1} l_1 = \frac{1 - \left(\frac{1 - c_1}{c_1} \right)^n}{1 - \left(\frac{1 - c_1}{c_1} \right)} l_1 \tag{3a}$$

and

$$L_n < \frac{1}{1 - \left(\frac{1 - c_1}{c_1} \right)} l_1 = L_\infty \tag{3b}$$

$$h = l_1 \frac{1 - (\frac{1 - c_1}{c_1})^n}{1 - (\frac{1 - c_1}{c_1})} \sqrt{1 - \frac{d^2}{c_1^2 l_1^2}} \sqrt{1 - \frac{d^2}{3 h_{\infty,d}^2}}$$

$$= L_n \sqrt{1 - \frac{d^2}{c_1^2 l_1^2}} \sqrt{1 - \frac{d^2}{3 h_{\infty,d}^2}}, h_{\infty,d} \geq \frac{d}{\sqrt{3}} \tag{4}$$

where

$$h_{\infty,d} = \frac{1}{1 - \left(\frac{1-c_1}{c_1}\right)}l_1\sqrt{1 - \frac{d^2}{c_1^2 l_1^2}} = \frac{c_1 l_1}{2c_1 - 1}\sqrt{1 - \frac{d^2}{c_1^2 l_1^2}}$$

(5)

Equation (3b) shows that, theoretically, for given $c_1 > 0.5$ the sum of length of elements cannot exceed some limit value L_∞, regardless of the number of elements n.

It is often the combination of slightly desynchronized dual or triple actuators that causes deviations from the predefined geometry and sets up undesirable residual stresses in the system (Adriaenssens and Ney, 2007). To avoid this phenomenon, the choice of pantographs as subsystems for the tetrahedral mast, is driven by the notion that the mast's vertical height can be controlled by manipulation of one degree of freedom only. This degree of freedom consists of the relative horizontal position (indicated in Figure 3 by the notation $2d$) of one support node with respect to the second, pinned support node provided the third support node is free to slide in the horizontal plane. The orientation of the displacement is defined by the first and second node. The use of one single actuator that moves one support toward or away from the second support allows for the controlled three-dimensional movement (as the mast increases its height, its width becomes smaller and *vice versa*). The mast height h can thus be expressed in terms of the distance between the two controlling support nodes $2d$, the number of scissors n, the ratio of the length between the bottom end node and the intermediate node to the length between the two end nodes c_1, and the length between the two end nodes of the bottom scissor element l_1, as shown in Equations (4) and (5).

Equation (5) represents the height of the triangle inscribed by the two-dimensional pantograph system (triangle formed by line ABCD, the base of the pantograph, and the line connecting the middle hinges). The first square root term in Equation (4) is the *sine* of the angle formed by the pantograph members with the two-dimensional base, and the second square root accounts for the tilting of a pantograph plane three dimensionally. Equations (3) and (4) point that for given L_n and n, the variables l_1 and c_1 cannot be independently selected, that is, they depend on each other.

The theoretical predefined maximum height of the mast h will occur for $d = 0$, and in this case it is equal to L_n, that is, $h(d = 0) = L_n$. The largest value of d is for two-dimensional pantograph equal to $c_1 l_1$, in which case $h = 0$. However, for three-dimensional tetrahedral pantograph, the condition that the hinges of three plane pantographs should be connected imposes that $h_{\infty,d} \geq d/\sqrt{3}$ (see Equation (4)). Consequently, the max-

imum d_{max} can be calculated from Equation (5) by solving equation $h_{\infty,d} = d/\sqrt{3}$, as shown in Equation (6)

$$d_{max} = c_1 l_1\sqrt{\frac{3}{3 + (2c_1 - 1)^2}}$$

(6)

For a nondeployed mast, the height is minimal (i.e., for a mathematically idealized mast the height is zero) and $d = d_{max}$. To adjust the height of the mast, the actuator changes the value of d. The stroke s of actuator is then defined as follows:

$$s = 2d_{max} - 2d, \; s_{max} = 2d_{max}$$

(7)

For given maximum value of h (i.e., L_n, see Equation (4), larger value of c_1 (closer to 1.0) implies larger d_{max} and consequently larger s_{max} and l_1 (see Equations (3), (6), and (7)). Large values of d_{max} and l_1 are not optimal as the footprint of the mast will be large and the individual beams of the pantograph will be long. When not deployed, the overall size of the mast will be large too and not compact enough to be transported (the longest length of beam l_1 will be too long). In addition, a large value of s_{max} requires a large stroke actuator. Contrary, for smaller values of c_1 (closer to 0.5), a nondeployed mast is very compact, and short-stroke actuator would be required. This discussion is illustrated by values for maximum element length, stroke, and height for a three-tiered tetrahedral mast in Table 1.

For example, the maximum beam length that can fit in a standard 40 ft. container is 12 m, which allows for a mast with three tiers of scissor elements and $c_1 = 0.55$ to have a maximum theoretical height of 27 m, approximately.

The relations between h and d, and h and s depend on the selection of l_1 and c_1, and their dependence is illustrated in Figure 4 for $n = 3$. Figures 4a and b show that coefficient c_1 does not significantly influence the relationship between h/L_n on one hand and $d/(2c_1 l_1)$ and $s/(2c_1 l_1)$ on the other hand.

However, the influence of the stroke on the height of the mast, that is, the influence of the ratio $s/(2c_1 l_1)$ to the ratio h/L_n can be roughly divided into three intervals:

1. The first interval corresponds to $s/(2c_1 l_1)$ ratio change from 0.00 to 0.05, approximately. These initially small changes of stroke produce large changes in height (h/L_n ratio changes from 0.0 to 0.3, approximately). Consequently small errors in stroke position can produce large errors in mast height.
2. The second interval corresponds to $s/(2c_1 l_1)$ ratio change from 0.05 to 0.60, approximately. This change of stroke produces a change in h/L_n

Table 1
Comparison of ratios between maximum length beam l_1, maximum stroke s_{max} and maximum theoretical height of mast L_n for masts with three scissor elements ($n = 3$) and various values of c_1

Parameter c_1 [−]	Max. length of a scissor beam l_1/L_n [−]	Max. stroke of a scissor beam s_{max}/L_n [−]
0.50*	0.33	0.33
0.55	0.40	0.44
0.60	0.47	0.59
0.70	0.62	0.87
0.80	0.76	1.22
0.90	0.89	1.60
1.00†	1.00	2.00

*Prismatic mast, not included in this research.
†Mast "collapsed" to hinged beams.

ratio from 0.3 to 0.9. This second stroke interval promises a better height control than the first stroke interval.

3. The third interval corresponds to $s/(2c_1l_1)$ ratio change from 0.60, approximately, to $s_{max}/(2c_1l_1)$. In this interval, a larger stroke is applied for very small gain in the mast height. This interval seems to promise the best control of the mast height is actually not optimum for two reasons: (1) large applied stroke requires a larger actuator, and (2) for a larger stroke the value d becomes very small and stability of the mast can be compromised.

In conclusion, based on the considerations above, the second interval seems to be the most suitable for active operation of deployed mast. This second interval was chosen for exploration when validating the physical model (see Section 3). Based on Table 1, the value of c_1 must be closer to 0.5 for a compact mast. However, this last requirement is in contradiction with the global stability and structural efficiency requirement, as shown in Subsections 2.2 and 2.3, respectively.

2.2 Global stability

Exposing the mast to lateral forces produces an overturning risk. In the preliminary study three load cases should be considered: (1) static loads due to the self-weight of the mast and the turbine, (2) the wind load, and (3) dynamic loads due to flow-induced vibrations of the wind turbine. The presented structure has a vertical axis wind turbine with three helically swept blades, which practically eliminates the turbine's dynamic effects on the mast (i.e., the cyclic aerodynamic loading of each blade's revolution) (Crosher and Cochrane, 2008). Consequently, only the first two load cases are considered. The horizontal forces acting on the mast are those generated by the wind pressure exerted on the turbine P (the turbine is modeled as a solid panel, and the value of P accounts for the dynamic amplification factor) and over the body of the mast $w(z)$ as illustrated in Figure 5a. The value of P and the distribution of $w(z)$ are determined by the strain sensors installed on the turbine support and pressure sensors installed on the mast scissor elements. Assuming that the mast is not anchored to the soil, the only force opposing the overturning is resultant $M + T$ that combines the weights of the mast M and turbine T ($T \approx$ 5–20% of M depending on material and size).
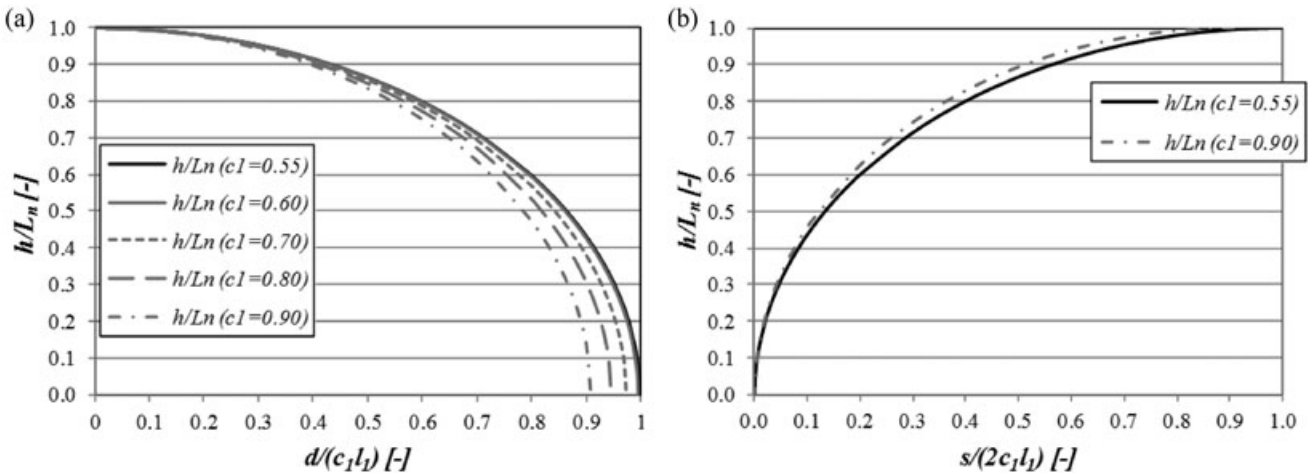

Fig. 4. (a) Relation between the relative height of the mast h and position d of the movable node for $n = 3$ and various values of coefficient c_1; (b) influence of the actuator stroke s to h for $n = 3$ and various values of c_1.
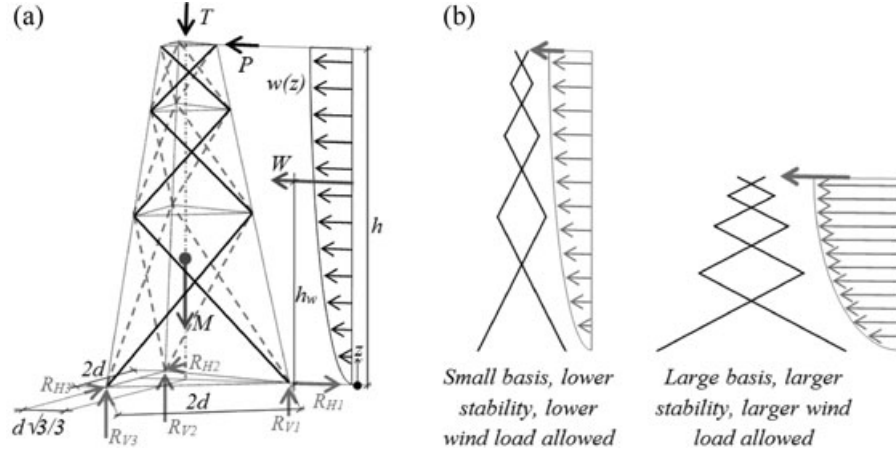
Fig. 5. (a) Simplified analysis of forces acting on mast and (b) adaptation to external forces improves stability.

By changing the height of the mast, two parameters are changed: (1) the wind load and the associated overturning moment are decreased, and (2) the footprint of the base is increased and consequently the resistance to overturning is improved as shown in Figure 5b.

The aim of this section is to assess how the coefficient c_1 influences the global stability of the mast. To simplify the presentation the influence of the wind blowing on the body of the mast, this load is replaced by its resultant W (multiplied with dynamic amplification factor A_w) acting at the centroid of the load, that is, at the height h_w. Values of W and h_w are thus calculated as follows:

$$W = A_w \int_0^h w(z)dz \text{ and } h_w = \frac{A_w \int_0^h w(z)zdz}{W} \quad (8)$$

To oppose the overturning the global moment due to the weight of the mast should not be smaller than the moment generated by the wind, that is

$$Ph + Wh_w \leq (M + T)d\frac{\sqrt{3}}{3} \quad (9)$$

Rearranging Equation (9) and combining with Equations (3) and (4) leads to

$$\frac{F}{G} \leq \frac{d}{h}\frac{\sqrt{3}}{3} = \frac{(2c_1 - 1)\frac{\sqrt{3}}{3}\frac{d}{c_1 l_1}}{\left(1 - \left(\frac{1-c_1}{c_1}\right)^n\right)\sqrt{1 - \frac{d^2}{c_1^2 l_1^2}}\sqrt{1 - \frac{d^2}{3h_{\infty,d}^2}}} \quad (10)$$

where $F = P + Wh_w/h$ is equivalent overturning force at the top of the mast calculated using sensor measurements and $G = M + T$ is total weight of the mast and turbine combined. This equation is used in control software algorithms to evaluate stability conditions of the mast.

The relationship between the upper limit of ratio F/G and value d and stroke s is given in Figures 6 and 7.
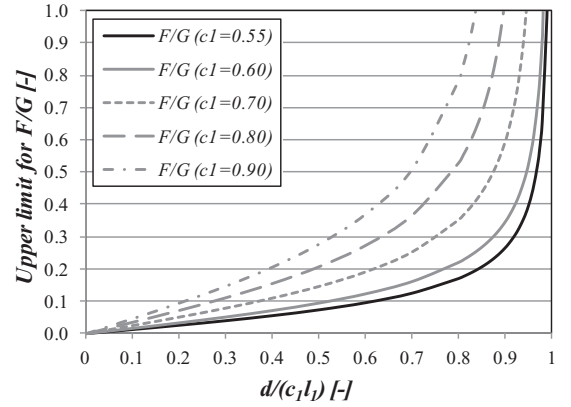

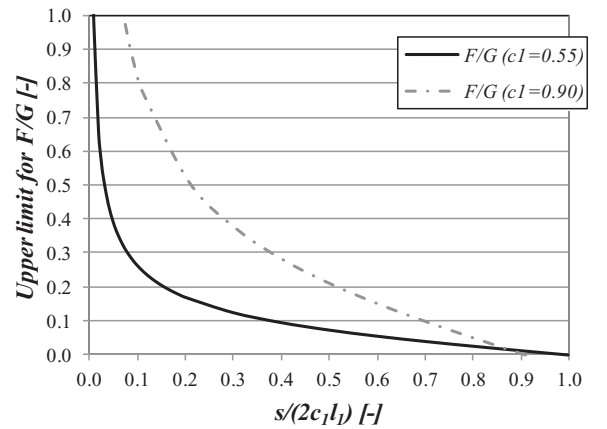**Fig. 6.** Relation between F/G ratio and d.

Fig. 7. Relation between F/G ratio and stroke s.

Figures 6 and 7 show that more stability is achieved if the value of c_1 is closer to 1.00. For example, assuming that two masts have the same weight, for a given stroke s the mast with $c_1 = 0.90$ will allow several times

a higher wind force on the turbine than the other one with $c_1 = 0.55$ (see Figure 7). An additional conclusion from Figure 7 is that an excessively large stroke will decrease stability of the mast, thus the stroke should be kept out of the third interval (see Subsection 2.1).

In conclusion, for global stability sake c_1 should be closer to 1.00. This finding is in contradiction with the compactness and controllability requirements that favor a short stroke (see Section 2.1). However, Equation (8) shows that by increasing the weight G of the mast it is possible to increase the stability against overturning and to allow for larger horizontal wind forces. In the case of a smart mast mounted on a steel shipping container (as the "Power in a Box" project) the mast can be additionally stabilized (its weight artificially increased) by the container in which the mast was transported and mounted (the weight of a 40' steel shipping container is 38 kN).

During folding and unfolding of the mast, the global stiffness of structure changes due to the overall change in geometrical shape. Although this change influences the displacement distribution along the mast, it does not affect the global stability of the structure, which only depends on parameters used in Equations (9) and (10).

2.3 Simplified structural analysis

The aim of this section is to analyze the relationship between the internal forces, the ratio c_1, the values of d, and stroke s. For the purpose of this preliminary design analysis, the load acting on the mast is divided into a vertical component (due to dead load and wind suction) and horizontal component due to wind. For each of the three pantograph systems the load can further be split into in-plane load (acting in the plane of pantograph) and out-of-plane load (acting perpendicular to the plane of pantograph). A detailed analysis of all loading combinations exceeds the scope of this section. To simplify the presentation, without reducing the validity of the general conclusions, only the analysis of internal forces generated by in-plane dead load is presented in detail. In the other load cases results leading to similar conclusions are obtained. In the analysis the pivot and end connections are assumed to be frictionless pins. Modeling of the friction in the joints is out of the scope of this study. The friction in the joints is found to amplify the horizontal forces for about 25% (e.g., Gantes et al., 1993). In the study of the full-scale prototype, it is assumed that the horizontal forces can be amplified by a factor of 1.25.

Each pantograph-tiered system is statically determinate in its plane and the loads flow from the top to the bottom. More precisely the load from the upper scissor element is transmitted to lower scissor element.
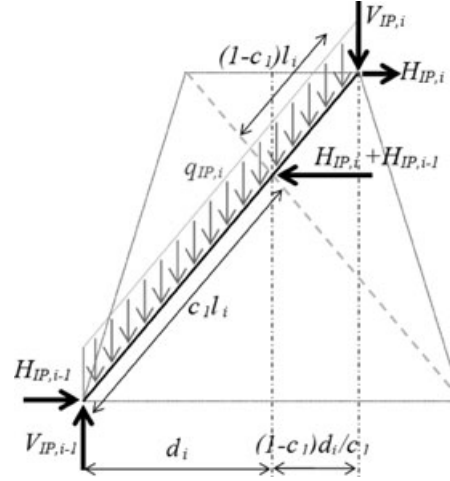

Fig. 8. Analysis of in-plane forces in ith element.

In addition the dead load is symmetric producing symmetric influences in two beams of the scissor element, and the vertical force in the hinge is equal to zero. Assuming perfect symmetry in dead load and in the pantograph's geometrical and mechanical properties, the in-plane load acting on the ith scissor element of a pantograph is transmitted only to the $i-1$st element of the same pantograph without affecting the other two pantographs in the tetrahedron. In-plane loads acting on ith scissor element are shown in Figure 8.

As the flow of the forces is from upper to lower scissors, the forces transmitted from the ith to $i-1$st scissor element are calculated using the following recursive formulas obtained from the equations of equilibrium

$$V_{IP,i-1} = V_{IP,i} + q_{IP,i}l_i \tag{11a}$$

$$
H_{IP,i-1} = \left(\frac{1-c_1}{c_1}\right)H_{IP,i} + \frac{1}{c_1}\frac{\frac{d}{c_1l_1}}{\sqrt{1 - \left(\frac{d}{c_1l_1}\right)^2}}V_{IP,i}
$$
$$
+ \frac{1}{2c_1}\frac{\frac{d}{c_1l_1}}{\sqrt{1 - \left(\frac{d}{c_1l_1}\right)^2}}q_{IP,i}l_i \tag{11b}
$$

where d_i/l_i is substituted with d/l_1 (see Figure 2), $i = 1$ to n, and index IP indicates in-plane load.

The recursive Equations (11a and b) can be rearranged as follows:

$$V_{IP,i} = V_{IP,n} + \sum_{j=i+1}^{n} q_{IP,j}l_j \tag{12a}$$

and

$$H_{IP,i} = \left(\frac{1-c_1}{c_1}\right)^{n-i} H_{IP,n}$$

$$+ \frac{1}{c_1} \frac{\frac{d}{c_1 l_1}}{\sqrt{1 - \left(\frac{d}{c_1 l_1}\right)^2}} \frac{\left(\frac{1-c_1}{c_1}\right)^{n-i} - 1}{\left(\frac{1-c_1}{c_1}\right) - 1} V_{IP,n}$$

$$+ \frac{1}{c_1} \frac{\frac{d}{c_1 l_1}}{\sqrt{1 - \left(\frac{d}{c_1 l_1}\right)^2}} \sum_{m=1}^{n-i-1} \frac{\left(\frac{1-c_1}{c_1}\right)^m - 1}{\left(\frac{1-c_1}{c_1}\right) - 1} q_{IP,i+m+1} l_{i+m+1} \qquad (12b)$$

$$+ \frac{1}{2c_1} \frac{\frac{d}{c_1 l_1}}{\sqrt{1 - \left(\frac{d}{c_1 l_1}\right)^2}} \sum_{m=1}^{n-i} \left(\frac{1-c_1}{c_1}\right)^{m-1} q_{IP,i+m} l_{i+m}$$

where $i = 0$ to $n - 1$.

Finally for dead load only, that is, $H_{IP,n} = 0$, constant value of distributed load, that is, $q_i = q_{IP} = constant$, and taking into account that in-plane load changes as the inclination of the pantograph changes with the parameter d (or stroke s, see also Equation (5)), Equation (12) transforms to

$$V_{IP,i} = \sqrt{1 - \frac{d^2}{3h_{\infty,d}^2}} \left(V_n + q \sum_{j=i+1}^{n} l_j\right) \qquad (13a)$$

where $V_{IP,n} = V_n \sqrt{1 - \frac{d^2}{3h_{\infty,d}^2}}$, $q_{IP} = q \sqrt{1 - \frac{d^2}{3h_{\infty,d}^2}}$ and

$$H_{IP,i} = \frac{1}{c_1} \frac{\frac{d}{c_1 l_1} \sqrt{1 - \frac{d^2}{3h_{\infty,d}^2}}}{\sqrt{1 - \left(\frac{d}{c_1 l_1}\right)^2}} \frac{\left(\frac{1-c_1}{c_1}\right)^{n-i} - 1}{\left(\frac{1-c_1}{c_1}\right) - 1} V_n +$$

$$\frac{1}{c_1} \frac{\frac{d}{c_1 l_1} \sqrt{1 - \frac{d^2}{3h_{\infty,d}^2}}}{\sqrt{1 - \left(\frac{d}{c_1 l_1}\right)^2}} \left[\frac{\left(\frac{1-c_1}{c_1}\right)^{n-i} - \left(\frac{1-c_1}{c_1}\right)}{\left(\frac{1-c_1}{c_1}\right)^2 - 1} + 2\right] q L_n$$

(13b)

Equation (13a) shows that the "vertical" in-plane force is minimal for $i = n$ (at the top of the mast) and gradually increases from the top to the bottom of the mast where it is maximum ($i = 0$, at the base). Equation (13b) shows that similar applies for the horizontal force. In Equations (12a and b), V_n corresponds to the weight of the turbine and q to the linear mass of the mast beams. For illustrative purposes, the relationship between d and the horizontal force at the base of the mast with three scissor elements ($n = 3$) for $V_n = 0.2qL_n$ (weight of turbine equals 20% of the weight of the mast, similar as for the full-scale prototype, see Section 3.1) normalized with total weight ($V_n + qL_n$) is given in Figure 9 for various values of parameter c_1.

Figure 9 shows that the horizontal reaction at the base of the mast increases with the increase of parameter d. The horizontal reaction increases as d approaches its maximum value (see Equation (6)), and then drops to zero when the mast collapses into a plane and reaches a critical configuration. The increasing horizontal reaction is more emphasized for smaller values of parameters $c_1 < 0.7$, especially for values $d/(c_1 l_1) > 0.85$. This observation is important as the horizontal support is moved by the actuator and large horizontal reaction requires a more powerful actuator.

Thus, during deployment, the mast cannot initially be raised from the collapsed horizontal state using the horizontal actuator, used to control the mast shape during the operation. Raising the mast from a horizontal state, needs an initial out-of-plane "kick" force. For example the actuator could temporarily be placed vertically in the center of the mast to raise the mast to its lowest operational height. Once the mast has achieved this height, it can be temporarily fixed (supports temporarily locked) and actuator can be placed in its operational horizontal position. Alternatively, two "permanent" actuators can be used, one to raise the mast and the other to operate it. In this case, these two actuators will operate completely independently, that is, the actuator that raises the mast to its lowest operational height can be disconnected once it has fulfilled its function. The use of two interchangeable actuators can also be justified to add redundancy to the systems (one actuator can be used for dual purpose if the other actuator fails).

For values of $d/(c_1 l_1) < 0.85$, that is, during the operation of the mast (see Section 2.1), the horizontal reaction is not excessively high. As the value $d/(c_1 l_1)$ will be higher than 0.85 only during the deployment of the mast, the smaller values of c_1 are acceptable, with the compromise that the lack in efficiency of the structure is compensated with a gain in compactness.

3 SMART TETRAHEDRAL PANTOGRAPH MAST: PHYSICAL PROOF OF CONCEPT

3.1 Initial target dimensions and performance

Based on the analysis presented in previous sections, it is possible to draft the target specifications for the smart tetrahedral mast. As the aim of this study is to prove the concept of the smart mast, only a simplified feasibility and performance assessment is made, while the development of design details are left for the second stage of the project. For transportation purposes, the mast should be collapsed and the mast sides disconnected along one imaginary edge of the tetrahedron and "folded" along the two other imaginary edges. In this folded and collapsed configuration, the three
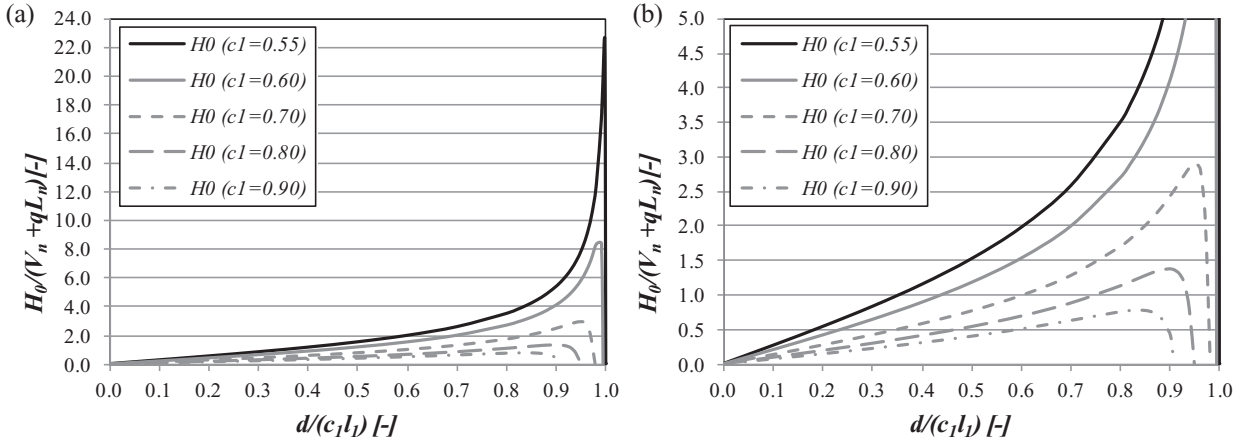
Fig. 9. (a) Relationship between d and the horizontal force at the base of the mast with three scissor elements ($n = 3$) for $V_n = 0.2qL_n$ normalized with total weight ($V_n + qL_n$); (b) detail from Figure to the left.

mast sides (each containing connected scissor elements) become parallel. To fit in a standard 40' shipping container, the size of the longest member should be defined so the value $2d_{max}$ does not exceed 10 m, keeping about 1 m space around the folded mast. Deployment from this compact form can be performed manually, with the help of the actuator (see Section 2.3). Based on the "Power in the Box" project, the minimum operating height is established around 10–12 m, and the maximum height around 18–20 m. The operating force in actuators should be kept relatively small 10–50 kN (equivalent to 1–5 tons), so the actuator will not have excessive power requirements. The mast can be made of thin-walled rounded rectangular steel profiles 50 × 150 × 4 mm. A vertical axis wind turbine with three helically swept blades, can be used, with weight of 4.5 kN and the projected peak power of 8.5 kW at wind speed of 16 m/s. Combining the drafted specifications with the research presented in Section 2, the initial target specifications are drafted as shown in Table 2.

At this stage of the research, it is difficult to accurately estimate the wind speed that will generate the maximum overturning moment. Wind tunnel test will be necessary for this purpose. Nevertheless, for the purposes of the study assuming drag coefficient of 2 and uniform distribution of the wind along the mast height (a conservative assumption), based on Equation (10), one can conclude that the mast can support wind gusts of 26 m/s. However, the true wind pressure will be actually measured by the pressure sensors (and not calculated from the wind speed). The control algorithms will have several criteria for adjusting the height of the mast: (1) to achieve optimal energy production efficiency, the mast will adapt its shape to tap into the optimal wind speed range (close to 16 m/s), (2) for the global stability, the

Table 2
The target specifications of the smart mast

n/c_1 [−]	3/0.55
Length l_1 [m]	9
Maximum theoretical height L_n [m]	22.4
Maximum operating height h_{max} [m]	$20.1 = 0.90L_n$
Minimal operating height h_{min} [m]	$11.9 = 0.53L_n$
Maximum stroke s_{max} [m]	9.9
Stroke at h_{max} $s(h_{max})$ [m]	$5.6 = 0.57(2c_1l_1)$ ($d = 2.1 = 0.43c_1l_1$)
Stroke at h_{min} $s(h_{min})$ [m]	$1.5 = 0.15(2c_1l_1)$ ($d = 4.2 = 0.85c_1l_1$)
Estimated weight with turbine (w. 40' container) G [kN]	25 (63)
Max. overturning moment at h_{max} (w. container) $M_{ot}(h_{max})$ [kNm]	53 (133)
Max. overturning moment at h_{max} (w. container) $M_{ot}(h_{min})$ [kNm]	104 (264)
Actuator force as per Section 2.3 at h_{max} $H_0(h_{max})$ [kN]	14
Actuator force as per Section 2.3 at h_{min} $H_0(h_{minx})$ [kN]	45

mast's height will change to ensure a satisfactory safety factor as per Equation (10), for example, for safety factor 2, $F/G < (2d\sqrt{3})/(3h)$, and (3) to reduce the power requirement, the actuator will move slowly and not in real time. Its movement will be controlled by thresholds based on 5–10 min wind-speed and pressure statistical analysis (averages and dispersion, e.g., Iglewicz and Hoaglin, 1993). A typical actuator speed of 1–5 m/min. (average power required 0.8–4 kW) is envisaged.
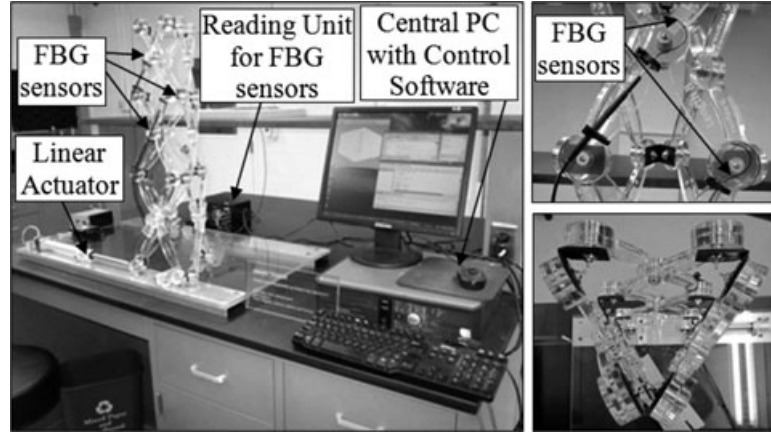
Fig. 10. (Left) View of smart mast with its control system; (upper right) detail of the scissor beam hinge; (lower right) detail of the inter-pantograph hinge (top view to the mast).

The actuator speed and the length of intervals for wind statistical analysis are site dependent and are determined based on historical data for each specific site. If the historical data show that the optimal height for the turbine does not vary significantly over time, and the wind gusts do not exceed the speed limit established for safe functioning of the mast, then the time intervals for the control system may be significantly elongated. However, it is not recommended to turn the control system off to be able to act upon extreme events that were rarely registered, or not registered in the history. In the cases where the historical data are missing, conservative values will be taken (higher safety factor, shorter time intervals for statistical data analysis, and faster movement of the actuator).

3.2 Description of the physical model

To prove the smart mast concept, a reduced-scale model was built and its responsiveness tested. The geometric scale of the model was adjusted to available material and equipment, and set to 1:27.5 with respect to target specifications given in Table 2. The model consisted of three two-dimensional pantographs, each made of three-tiered connected scissor elements that decrease in size (see Figure 10). The dimensions of the model were chosen based on geometrical stability and structural analysis presented previously in Section 2. It is composed of 18 laser-cut 9-mm thick acrylic beams. As acrylic has lower density than steel, these beams are widened and thickened to account for the concentrated force transfer in the hinged connection at the beam extremities and at the intermediate hinges. Each scissor unit is made of two identical members hinged together using a stainless steel rotational hinge (see Figure 10). The extremities of the different tiers of scis-

sor elements are connected with a similar type of planar rotational stainless steel connection. The three pantographs are connected at the beam extremities using a folded rubber hinge (see Figure 10). The resulting weight of the mast was 24 N (mass of 2,436 g). Thus, the scale of the weight with respect to target values was approximately 1:1,000, which was a direct consequence of lower density of acrylic (6.6 times compared with steel), shorter lengths, and smaller cross-section. Lower strength of acrylic resulted in larger area of the scissor elements, and thus the aerodynamics properties of the model would not be representative for the targeted mast. However, as the wind tunnel tests were out of the scope of this study, this matter did not affect the overall presented results. The mast model rests on three supports: the first is pinned in all directions, the second can slide along one direction (along the stroke of the actuator), but it cannot slide in the perpendicular direction, and the third support is free to slide in all directions. The two sliding base supports displace over a Teflon coated surface and ensure that during displacement those supports do not encounter frictional resistance and thus do not induce extra stresses in the model. Table 3 presents the main characteristics of the model.

3.3 Control system

The mast model is equipped with a smart control system, that is, with a sensing system, actuator, and data processing subsystem shown in Figure 10.

The sensing system consists of three Fiber Bragg-grating (FBG) sensors for temperature monitoring (simplification made to use readily available material, see Subsection 1.1), reading unit, and associated interface software. The error limits of the system were $\pm 0.2°C$ in short term and $\pm 0.5°C$ in long term. The

Table 3
The main characteristics of the smart mast physical model

n/c_1 [−]	3/0.55
Length l_1 [mm]	327
Maximum theoretical height L_n [mm]	813
Maximum operational height h_{max} [mm]	$736 = 0.90L_n$
Minimal operational height h_{min} [mm]	$429 = 0.53L_n$
Maximum stroke s_{max} [mm]	360
Stroke at h_{max} $s(h_{max})$ [mm]	$207 = 0.57(2c_1l_1)$ $(d = 77 = 0.43c_1l_1)$
Stroke at h_{min} $s(h_{min})$ [mm]	$55 = 0.15(2c_1l_1)$ $(d = 153 = 0.85c_1l_1)$
Weight G [N]	24
Max. overturning moment at h_{max} $M_{ot}(h_{max})$ [Nm]	51
Max. overturning moment at h_{max} $M_{ot}(h_{min})$ [Nm]	101
Horizontal force as per Section 2.3 at h_{max} $H_0(h_{max})$ [N]	13
Horizontal force as per Section 2.3 at h_{min} $H_0(h_{min})$ [N]	43

frequency of measurements was 1 kHz. The sensors were installed at hinges of scissor elements No. 2 and 3, and at interpantograph hinge of these two scissor elements (see Figure 10). The acquired data were stored in the form of text-files on a central PC. Simulation of wind pressure sensors by temperature sensors is justified by the fact that the numerical outputs are the same for both types of sensors (i.e., scalar value for each instrumented point).

A single linear actuator provided the mast with its kinematics. The actuator has a maximum stroke of 203.2 mm (8 in.), high torque 17 stepper motor, and thrust to 1.78 kN (400 lbs.), and it operates on its own power unit. The total stroke of available actuator is shorter than the one required for full deployment (360 mm, see Table 3), but sufficient for the operation (operational range was 207–55 = 152 mm). The interface software was installed on a central PC that also controls the actuator. The speed of the actuator was adjusted to draft target value.

A MatLab-based Control Software (MathWorks, Inc., Natick, MA, USA) was created and uploaded on the central PC. The program processes the data acquired by sensors, makes an analysis, and sends control information to the actuator, so the latter can induce shape change of the mast. A simple Java-based routine allows for integration of various interfaces (sensors and actuator) and Control Software, and provides a fully au-tomatic operation of the control system (sensing, processing, actuation).

A change in temperature for a minimum averaged difference of 5°C for period not shorter than five seconds (statistical analysis interval, total of 5,000 measurements) at any location or any combination of locations ("area") equipped with sensors (that simulates excessively strong wind at that location or that area) results in movement of the top of the mast to that location. The idea being that the mast equipped with wind turbines installed at its top would try to avoid "strong wind" over its body, still keeping the turbine in the acceptably strong wind. The interrogation period of five seconds was set to be short so the tests can be performed quickly, by blowing, still collecting a large amount of measurements that are statistically analyzed. The speed of actuator was set to 5 mm/s, so the full movement is achieved within 30 seconds. With this speed no visible dynamic effects were noticed due to actuation.

3.4 Shape changing sequence

Figure 11 illustrates how the tetrahedral pantograph reduced-scale physical model responds to the external stimulus of temperature by shifting its shape in a stable manner. Upon sensing a change in temperature (human breath) at one or several sensors, the mast contracts so that its top is at the level of initial location of the lowest activated sensor. When the temperature difference is removed, the mast expands to initial deployed position.

4 CONCLUSIONS AND FUTURE WORK

This article presents progress in the field of smart civil structures by investigating an adaptive tetrahedral pantograph mast with potential application in the domain of disaster relief and recovery infrastructure. Key design criteria in this context are compactness (for transportation), deployability (for ease of erection), responsiveness (adaptability to changing and unknown external boundary conditions such as loading), and global stability (in absence of guy lines in a restricted site).

The project has been developed in two phases, and the first phase is presented in this article, while the second phase represents the topic of the future work. The major fundamental questions on feasibility of a tetrahedral pantograph mast and the proof of concept are addressed, including the studies on the change of shape under external influences, global stability requirements, structural analysis of the mast during the deployment, and a physical concept validation.
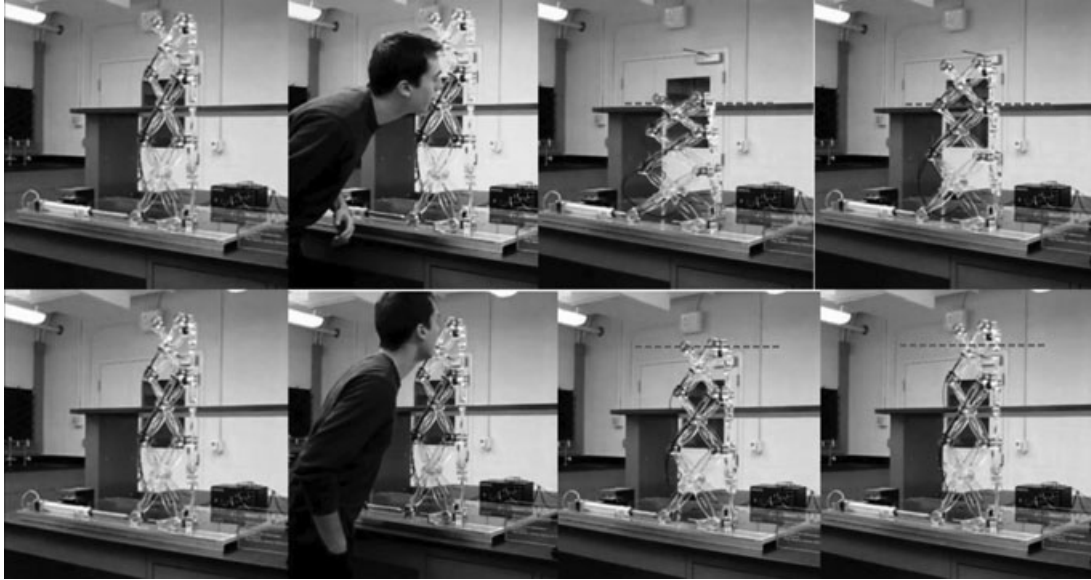
Fig. 11. Contraction and deployment sequence of the small-scale pantograph smart mast reacting to temperature differences, sensed at the element extremities.

The following are the contributions that to the best of the authors' knowledge have not been presented in earlier research:

1. The study considers deployable mast with a tetrahedral global form made up of scissor elements that do not have intermediate pivot hinge in the middle of the beams;
2. The kinematics of the tetrahedral mast were derived taking into account the change in inclination of the planes of scissor elements as the mast changes shape;
3. The structural analysis of this particular scissor element is performed taking into account the change in inclination of the element plane; analytical expressions are derived in closed form;
4. A simplified analysis of stability under the wind load was performed, and stability criterion established taking into account the variable height of the mast;
5. A physical smart mast model, equipped with sensors and actuators, was created to prove the concept.

Based on the case study of a tetrahedral three-tiered mast, the article derives the geometrical relationship based on deployability criteria between scissor beam length on one hand and mast height and actuator stroke length on the other hand for a range of intermediate hinge locations. The results of this analysis further show that the effect of the actuator stroke on the to-tal height does not significantly depend on the position of the intermediate scissor hinge. However, when deployed from a compact state, small changes in stroke length generate large initial increases in mast height. In a second interval, further increases in stroke length result in smaller gains in mast height. This interval is favorable when exercising control over the deployment is important. A third stroke interval exhibits large actuator strokes with very small mast height increase.

Geometrically, the most compact mast requires its intermediate hinge to be positioned close to midway between the beam's extremities. Analytical global stability expressions demonstrate that this compactness ideal is in contradiction with requirements for preventing overturning. However, the overturning can be prevented by increasing the weight of the mast by container used for its transportation.

A structural analysis at element level investigates the flow of forces and evaluates the horizontal base component that needs to be resisted by actuator during all phases of deployment. The actuation force required to lift or to collapse the mast is of interest as it directly relates to the structural and operational efficiency and cost of the smart mast. As expected, the horizontal actuation force increases nonlinearly as the mast lowers and approaches its maximum value just before dropping off to zero when attaining a theoretical horizontal compacted state. The increase in actuation force is more pronounced for more compact designs (where the intermediate hinge is close to the middle location of the scissor beam). For the established intermediate

favorable control stroke interval, the required actuation force proves to be acceptable.

To validate the practical feasibility of the structure, its kinematics and responsiveness, a small-scale acrylic three-tiered prototype equipped with a smart control system was designed, constructed, and extensively tested. Its control system consisted of (1) FO sensors with associated reading unit and interface software, (2) an actuator with associated interface software, (3) an original MatLab-based Control Software created upon the theoretical equations presented in the article, and (4) an original Java routine that integrated various interfaces and Control Software and provided with a fully automatic operation. Interpretation of the analysis and physical experimentation yields practical conclusions that can inform preliminary design decisions for a vast range of smart pantograph mast geometries.

The main limitations of the presented study are related to lack of simulations of real site conditions, namely the dynamic effects of wind, influence of displacements of the top of the mast to serviceability of the turbine, and the influence of friction in hinges and supports to the force distribution in the scissor elements and to the power requirements of the actuator. The realization of hinges may be challenging, as they are supposed to allow rotations between elements in two scissor planes, but also rotations between these two planes with minimal friction. Finally, an optimal sensor network allowing an accurate mapping of wind forces (as per Equation (8)) and robust algorithm that govern the mast deployment and adaptability should be developed and tested. All these challenges should be addressed in the future second phase of the project. The validation should include testing of scaled model in a wind tunnel and a large-scale testing on-site.

The presented analysis and the physical experimentation suggest future avenues of research related to full-scale robustness, kinematics and control framework. In particular detailed global stability under the wind, realization of details, power consumption, and robust control system will be addressed in the future research.

ACKNOWLEDGMENTS

REFERENCES

Adam, B. & Smith, I. (2008), Active tensegrity: a control framework for an adaptive civil-engineering structure, *Computers and Structures*, **86**(23–24), 2215–23.

Adriaenssens, S. & Ney, L. (2007), The piston-stayed bridge: a novel typology for a mobile bridge at Tervate, Belgium, *Structural Engineering International*, **17**(4), 302–05.

Aldemir, U. (2010), A simple active control algorithm for earthquake excited structures, *Computer-Aided Civil and Infrastructure Engineering*, **25**(3), 218–25.

Bitaraf, M., Hurlebaus, S. & Barroso, L. R. (2012), Active and semi-active adaptive control for undamaged and damaged building structures under seismic load, *Computer-Aided Civil and Infrastructure Engineering*, **27**(1), 48–64.

Cai, Z., Zhao, H. C., Zhao, J. S. & Chu, F. L. (2012), Stiffness of a foldable tower for wind turbine, *The Open Mechanical Engineering Journal*, **6**(Suppl 1-M4), 50–64.

Chen, W. J., Fu, G. Y., Gong, J. H., He, Y. L. & Dong, S. L. (2002), Dynamic deployment simulation for pantographic deployable masts, *Mechanics of Structures and Machines*, **30**(2), 249–77.

Ching, K., Liu, S. & Li, J. (2008), *Intelligent Structures*, Elsevier Science Publishers Ltd., UK.

Crosher, S. & Cochrane, R. (2008), qr5, Vertical Axis Wind Turbine, Vibration Characteristics, factsheet C.034, quietrevolution ltd., London. Available at: http://www.quietrevolution.com, accessed October 10, 2012.

Del Grosso, A. & Basso, P. (2011), A finite state strategy for the control of adaptive structural envelopes, in *Proceedings of the 22nd International Conference on Adaptive Structures and Technologies*, Paper #072, Corfu, Greece.

Escrig, F. (1985), Expandable space frame structures, in *Proceedings of Third International Conference on Space Structures*, Guildford, UK, 845–50.

Escrig, F. (2001), Geometry and structures: historical impressions about architecture, *Journal of Association of Shell and Spatial Structures*, **52**(1), 25–38.

Freedman, D. (1991), Invasion of insect robots, *Discover*, March, 42–50.

Gantes, C., Connor, J. J. & Logcher, R. D. (1993). Simple friction model for scissor type mobile structures. *Journal of Engineering Mechanics*, **119**(3), 456–75.

Gantes, C. J. (2001), *Deployable Structures*, MIT Press, Boston, MA.

Ghodrati, A. (2002), Seismic sensitivity indicators for tall guyed telecommunication towers, *Computers and Structures*, **80**(3, 4), 349–64.

Glisic, B. & Inaudi, D. (2007), *Fibre Optic Methods for Structural Health Monitoring*, John Wiley & Sons, Chichester, UK.

Glisic, B., Inaudi, D., Kronenberg, P., Lloret, S. & Vurpillot, S. (1999), Special sensors for deformation measurements of different construction materials and structures, in *Proceedings of SPIE – The International Society for Optical Engineering*, Newport Beach, CA, **3670**, 505–13.

Hoberman, C. (1990), *Reversibly Expandable Double-Curved Truss Structures*, US Patent 4942700.

Hunt, J., Haase W. & Sobek, W. (2009), A design tool for spatial tree structures, *Journal of the International Association of Shell and Spatial Structures*, **50**(1), 3–10.

Iglewicz, B. & Hoaglin, D. (1993), *How to Detect and Handle Outliers,* ASQC Quality Press, Milwaukee, WI.

Inaudi, D. & Glisic, B. (2002), Development of a fiber-optic interferometric inclinometer, in *Proceedings of SPIE – The International Society for Optical Engineering*, San Diego, CA, **4694**, 36–42.

Inaudi, D. & Glisic, B. (2006), Reliability and field testing of distributed strain and temperature sensors, in *Proceedings of SPIE – The International Society for Optical Engineering*, San Diego, CA, **6167**, 61671D-1–61671D-8.

Inaudi, D., Glisic, B., Fakra, S., Billan, J., Perez, J., Redaelli, S. & Scandale, W. (2001), Development of a displacement sensor for the CERN-LHC superconducting cryodipoles, *Measurement Science and Technology*, **12**(7), 887–96.

Jiang-Pin, J. & Dong-Xu, L. (2010), Optimal placement and decentralized robust vibration control for spacecraft smart solar panel structures, *Smart Materials and Structures*, **19**(8), 1–9.

Kar, D. (2003), Design of a statically stable walking robot, *Journal of Robotic Systems*, **20**(11), 671–86.

Kim, H. & Adeli, H. (2004), Hybrid feedback-least mean square algorithm for structural control, *Journal of Structural Engineering, ASCE*, **130**(1), 120–27.

Kim, H. & Adeli, H. (2005a), Hybrid control of smart structures using a novel wavelet-based algorithm, *Computer-Aided Civil and Infrastructure Engineering*, **20**(1), 7–22.

Kim, H. & Adeli, H. (2005b), Wind-induced motion control of 76-story benchmark building using the hybrid damper-tuned liquid column damper system, *Journal of Structural Engineering, ASCE*, **131**(12), 1794–802.

Kwan, A. (2003), A pantographic deployable mast, Ph.D. thesis, University of Cambridge, UK.

Long, G. & Collins, C. (1992), A pantograph linkage parallel platform master hand controller for force-reflection, in *Proceedings of the International Conference on Robotics and Automation*, Nice, France, 390–95.

Moorhouse, D., Sanders, B., Von Spakovskym, M. & Butt, J. (2006), Benefits and design challenges of adaptive structures for morphing aircraft, *Aeronautical Journal*, **110**(1105), 157–62.

Noak, T., Ruth, J. & Muller, U. (2006), Adaptive hybrid structures, in *Proceedings of International Conference on Adaptable Building Structures*, Eindhoven, The Netherlands.

Park, T., Han, C. & Jang, J. (2003), Dynamic sensitivity analysis for the pantograph of a high-speed rail vehicle, *Journal of Sound and Vibration*, **266**(2), 235–60.

Pawlowski, P. & Holnicki-Szulc, J. (2004), Adaptive structures under extreme loads – impact detection, self-adaptation, self-repairing, in *Proceedings of the Third International Conference on Structural Control*, Vienna, Austria.

Pellegrino, S. & Kwan, A. S. K. (1991), The pantographic deployable mast: design, structural performance and deployment tests, in *the Proceedings of the Conference on Mobile and Rapidly Assembled Structures* (MARAS 91), Southampton, UK, 213–24.

Peters, C. (2012), Power in a box: shipping sustainable energy to recovering and off-the-grid communities. Available at: http://powerbox.princeton.edu/, accessed on June 18, 2012.

Pinero, E. (1965), *Three Dimensional Reticular Structure*, US Patent 3185164.

Pinet, E., Hamel, C., Glisic, B., Inaudi, D. & Miron, N. (2007), Health monitoring with optical fiber sensors: from human body to civil structures, in *Proceedings of SPIE – The International Society for Optical Engineering*, San Diego, CA, **6532**, doi: 10.1117/12.715186.

Saleh, A. & Adeli, H. (1998), Optimal control of adaptive/smart building structures, *Computer-Aided Civil and Infrastructure Engineering*, **13**(6), 389–403.

Tan, G. E. B. & Pellegrino, S. (2008), Nonlinear vibration of cable-stiffened pantographic deployable structures, *Journal of Sound and Vibration*, **314**(3–5), 783–802.

Thrall, A. (2011), Design and optimisation of linkage-based movable bridge forms, Ph.D. thesis, University of Princeton, NJ.

Yao, J. (1972), Concept of structural control, *ASCE Journal of Structural Division*, **98**(7), 1567–74.

You, Z. & Pellegrino, S. (1997), Foldable bar structures, *International Journal of Solids and Structures*, **34**(15), 1825–47.

Zeigler, T. (1976), *Collapsible Self Supporting Structures*, US Patent 3968808.

Zhao, J. S., Chu, F. & Feng, Z. J. (2009), The mechanism theory and application of deployable structures based on SLE, *Mechanism and Machine Theory*, **44**(2), 324–35.

Zhao, J. S., Wang, J. Y., Chu, F., Feng, Z. J. and Dai, J. S. (2011), Structure synthesis and statics analysis of a foldable stair, *Mechanism and Machine Theory*, **46**(7), 998–1015.

Zuk, W. & Clark, R. (1970), *Kinetic Architecture*, Van Nostrand Reinhold Company, London.